Rayleigh-Brillouin spectra of the solid electrolyte $RbAg_4I_5$

Robert A. Field,* David A. Gallagher,† and Miles V. Klein
Department of Physics and Materials Research Laboratory, University of Illinois at Urbana-Champaign, Urbana, Illinois 61801
(Received 8 March 1978)

The low-frequency Raman spectra and the Rayleigh-Brillouin spectra of the crystalline electrolyte, rubidium silver iodide have been measured. At 90°C the longitudinal-acoustical phonon was observed by Brillouin scattering with a triply-passed Fabry-Perot interferometer to have a frequency consistent with known and measured physical properties of the crystal. The absolute intensity was compared with that of fused silica, yielding a value for the Rayleigh ratio of 2×10^{-6} cm^{-1} and for the Pockels' coefficient of 0.15. The Brillouin linewidth was instrumental and less than 0.3 GHz. The Rayleigh-Brillouin spectra were dominated by an intense Rayleigh peak of width less than 10 MHz and Rayleigh ratio of 0.14 cm^{-1}. Removal of this feature with an iodine filter revealed a dynamic central peak wider than the 350-MHz half-width of the filter. Analysis and comparison between data from an interferometer and a double monochromator lead to the conclusion that the central peak may be described as a sum of two Lorentzians. The narrower peak has a half-width of roughly 9 ± 3 GHz and a Rayleigh ratio of 4×10^{-6} cm^{-1}. Its width is consistent with a relaxation rate estimated from the diffusivity. The broader peak has a half-width of 40 ± 6 GHz and a Rayleigh ratio of about 9×10^{-7} cm^{-1}. Its origin is less certain, but it may be a measure of the time of flight of mobile silver ions.

I. INTRODUCTION

Rubidium silver iodide ($RbAg_4I_5$) has the highest ionic conductivity, 0.25 $(\Omega\,\mathrm{cm})^{-1}$, at room temperature of all measured solids and is therefore one of the most interesting examples of a solid electrolyte.[1] Such materials possess a high-temperature electrolyte phase in which one or more ionic sublattices remains rigid while another ionic sublattice becomes very disordered. The ions in the disordered sublattice can occupy many more sites than there are available ions, and the activation energy for transitions among sites is small.[2] Consequently these ions are highly mobile and are responsible for the fast ion conduction,

We report here a measurement of the longitudinal acoustical Brillouin spectrum along with a study of the motions of the mobile silver ions in $RbAg_4I_5$ using inelastic-light-scattering techniques. The frequency range of particular interest is 10^9–10^{11} Hz. This is where one expects to observe individual ion hopping processes, based on estimates of the mean time of stay, or dwell time from diffusivity measurements. In the remainder of the Introduction we review some relevant previous work and discuss briefly the nature of Rayleigh scattering expected in a solid electrolyte.

In the room temperature or α phase of $RbAg_4I_5$ the silver cation sublattice is disordered, and the iodine-anion sublattice is arranged to provide a large ratio of available sites to the number of available mobile cations.[3] These sites are connected by networks of passageways due to the sharing of faces between neighboring anion polyhedra. $RbAg_4I_5$ has four formula units per unit cell. The 20 iodine anions are arranged as in β-manganese so as to provide four distorted octahedra for the 16 silver cations. The tetrahedra consist of three sets of crystallographically nonequivalent sites. There are eight type-I sites, whose fractional occupation is 0.11. There are 24 type-II and 24 type-III sites with fractional occupations of 0.39 and 0.23, respectively. The face-sharing of the type-II and -III site polyhedra forms channels through which the silver cations can zig-zag. There are two channels perpendicular to each unit-cell face. Face sharing of type-I and -II sites provides cross links between channels. All of the sites of a particular type have the same energy but the orientations of the tetrahedra may be different so that the polarizability of a cation may change even if it hops between two sites of the same type.

Below 300 K $RbAg_4I_5$ is thermodynamically unstable against formation of AgI and Rb_2AgI_3.[4] We have found, however, that crystals of $RbAg_4I_5$ remained optically clear for two years when kept in a dry atmosphere below 300 K. However, at any temperature in the presence of water vapor the crystals will decompose significantly in a few hours to a month, depending on the humidity. The transparent crystals normally are tinted yellow and have a bandgap of 3.0 eV,[5] which implies they are unstable for wavelengths near or shorter than 4100 Å. At 5145 Å the crystals suffered surface damage in the form of pits and dark regions upon a few hours exposure to several milliwatts of focussed laser light. However, decomposition was observed by us even under laser irradiation at 6471 Å.

Previous polarized Raman studies on $RbAg_4I_5$ have revealed three features[6]: (i) a broad peak

at 105 cm^{-1} strongest in A_1 symmetry that was assigned to motions of the iodine tetrahedra, primarily of a breathing character; (ii) a broad peak near 20 cm^{-1} (with some finer structure) present only in E and T_2 symmetry that was assigned to the "attempt vibrations" of the Ag^+ ions within their tetrahedral iodine cages; and (iii) a rise below 8 cm^{-1} in A_1, E, and T_2 symmetries suggesting the tail of an inelastic Rayleigh peak due to the diffusional, hopping motion of the Ag^+ ions. A systematic study of the first two features is the subject of a separate paper.[7] The present work provides more information on the lowest frequency feature. Since the rate of hopping apparently corresponds to a frequency of a few cm^{-1} or less, there is a good chance in $RbAg_4I_5$ of affecting a rather clear separation between hopping of silver ions among sites and vibration of the ions at sites.

When an ion hops among sites of low local symmetry the local polarizability associated with the ion will fluctuate. This will lead to scattering of light in the form of Rayleigh scattering, which should consist of polarized scattering due to ions hopping among inequivalent sites of unlike polarizabilities plus depolarized scattering due to ions hopping among sites that are anisotropic although energetically equivalent. One can calculate the light scattering in the dilute limit in terms of the "relaxation modes" of a single fast ion.[8] Details are given in the Appendix. Coupling to strains has been considered for the case that the relaxation mode has a two-well character (pseudospin).[9] A properly symmetrized linear combination of such "spins" having T_2 symmetry is probably the order parameter of the 208-K phase transition in $RbAg_4I_5$.[10] We had hoped to be able to observe critical slowing down of this T_2 relaxation mode as 208 K is approached from above, but we were unable to obtain spectra of any quality below room temperature.

Of relevance for the present work is a recent low-frequency Raman study on α-AgI, where at 178°C the spectrum near zero-frequency shift was interpreted as the sum of broad and narrow Rayleigh components.[11] A fit was made with Lorentzians of half width 32 and 3.8 cm^{-1}, respectively. The broad Rayleigh wing was attributed to diffusive motions of the mobile silver ions, and the narrow component was attributed to the hopping motion of the ions among neighboring interstitial sites.

II. EXPERIMENTAL

A crystal of $RbAg_4I_5$ of irregular shape and dimensions of 1–3 mm was grown, cut, and polished.[6,7] The growth method was that of Manning et al.[12] and involves evaporation of a saturated hydrogen iodide solution. These crystals are superior in optical quality to those grown by other methods and produced the first polarized Raman spectra.[6] The required faces, two (110) and one ($\bar{1}10$), where cut by grinding the easily crumbled crystal gently with dry 600 grit sand paper. Fine polishing was with 1 μm diamond past on a microcloth without lapping oil. The crystal was then mounted in an optical cell that was flushed with dry nitrogen and had a heater and thermocouple to maintain temperatures between 300 and 370 K.

The light was incident along the [110] direction and was scattered into the [$1\bar{1}0$] direction. The polarization direction V ("vertical" with respect to the scattering plane) was along [001], and the polarization direction H for the scattered proton was along [110]. With regard to Raman polarization selection rules for O symmetry, VV spectra give a superposition of symmetries weighted as $A_1+\frac{4}{3}E$, and VH spectra have T_2 symmetry. With regard to selection rules for Brillouin spectra, the scattered phonon propagates along [100]; the VV spectrum should couple to the longitudinal phonon with an intensity proportional to the square of the Pockels coefficient P_{12}; the VH spectrum should couple to the transverse phonon with an intensity proportional to $\frac{1}{2}P_{44}^2$.

Four experimental methods were used to gain information about the low-frequency light scattering spectra. Figure 1 shows the optical arrangement for high-resolution high-contrast studies of the Rayleigh-Brillouin spectra using a triple-pass plane-parallel Fabry-Perot interferometer (PPFP) and a custom-made double grating monochromator. Typically the Fabry-Perot had a 60-GHz free spectral range, a finesse of 50, and a contrast of at least 2×10^6. The monochromator was set at the laser line and had a 1-cm^{-1} bandpass. A single-mode argon-ion laser was focused onto the crystal which was mounted in a nitrogen gas filled chamber and was kept above the 27°C disproportionation temperature.

The retroreflecting cube corners were removed to perform studies with a single-pass Fabry-Perot. An iodine absorption cell was placed in the collimated beam before the interferometer. Light-gathering power was thereby gained, and the reduced resolution and contrast were acceptable in the absence of the intense Rayleigh peak.

Observation of the unattenuated Rayleigh peak at very high resolution was obtained by replacing the interferometer in the brass box of Fig. 1 by a confocal spherical Fabry-Perot interferometer (CSFP) that had a 2-GHz free spectral range, a

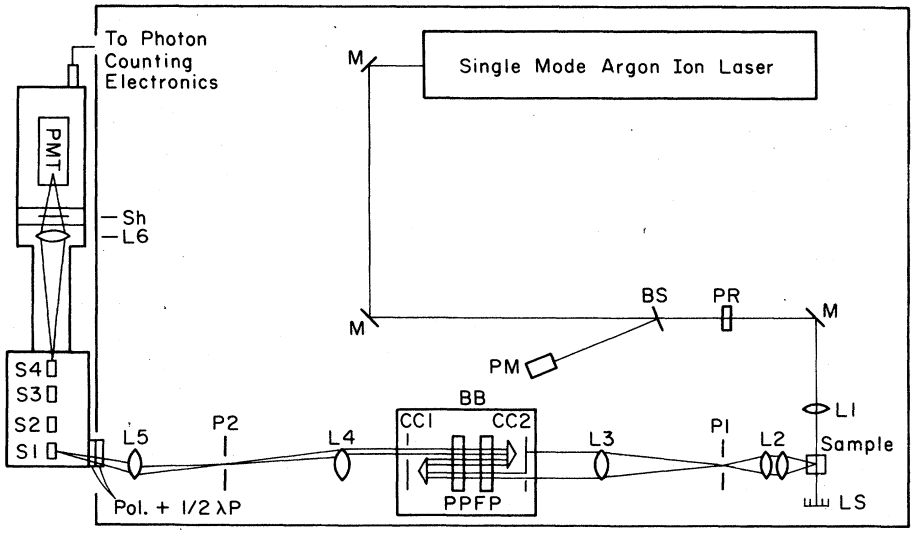

FIG. 1. Experimental arrangement of the triple-pass plane-parallel Fabry-Perot interferometer and double monochromator for 90° scattering. CC1 and CC2, cube corner retroreflectors; M, mirror; BS, beam splitter; PM, power monitor; PR, polarization rotator; $L1$, focusing lens; LS, laser stop; $L2$, two lens relay (100 mm each); $P1$ and $P2$, pinholes; $L3$, collimating lens (330 mm); BB, insulated brass box; $L4$, decollimating lens (330 mm); L5, offset relay lens (115 mm); Pol., polaroid; $\frac{1}{2}\lambda P$, half-wave plate; $S1$–$S4$, monochromator slits; $L6$, photocathode focusing lens (2.5:1); Sh, shutter; PMT, photomultiplier tube.

finesse of 70 and a contrast of 6000.

For the Fabry-Perot work (triple-pass PPFP and CSFP) in which no iodine cell was used, the microcomputer-based system developed by Wood[13] was used to stabilize the interferometer. When the iodine cell was used the system was not stabilized and was manually checked frequently.

Measurements were also made with a standard Raman scattering apparatus using an iodine cell and a Spex model 1400 $\frac{3}{4}$-m Czerny-Turner double-grating monochromator, equipped with 1200-groove/mm ruled gratings blazed at 1 μm and used in second order. The spectrum from 0 to 10 cm^{-1} was recorded with 0.6 cm^{-1} resolution. The Brillouin doublet was resolved from the central peak with 0.25 cm^{-1} resolution. This required a mask inside the monochromator to decrease aberrations of the slit image by reducing the solid angle, thereby reducing the instrumental slit width to within a factor of four of the diffraction limit.

Whenever the iodine cell was used, the single-mode laser was tuned to the 5145-Å absorption line of molecular iodine.[14] The 80-mm-long cell was observed to attenuate the laser beam by a factor of 5×10^8 when the iodine temperature was 95°C. Due to the sensitivity of the crystals to deterioration upon exposure to laser light, the laser power did not exceed 10 mW and often was 1 mW.

III. RESULTS

A. Triply-pass Fabry-Perot interferometer

Figure 2 shows the intense Rayleigh Peak and the Brillouin doublet located at ± 10 GHz in $RbAg_4I_5$. The peaks in the doublet occur at frequencies that satisfy the relation

$$f_q = \pm 2f_0(nv_q/c)\sin(\tfrac{1}{2}\theta)\,. \qquad (1)$$

Here c is the speed of light, $\theta = 90°$ is the scattering angle, f_0 is the frequency of the incident 5145-Å light and $v_q = 1.75\times10^5$ cm/sec is the speed of a LA phonon propagating in a ⟨100⟩ direction.[15,16] We determined the value of the refractive index to be $n = 2.1$ by measuring the apparent thickness of

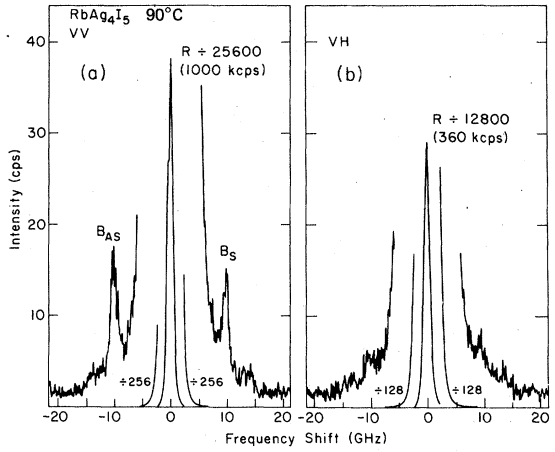

FIG. 2. Triple-pass PPFP data of $RbAg_4I_5$ at 90°C. In this and subsequent figures the abscissa is the amount of downshift of the scattered photon. The ordinate is photomultiplier counts per second. R denotes the Rayleigh peak; B_S and B_{AS} denote the Stokes and anti-Stokes Brillouin peaks, respectively. (a) 90° VV scattering. Rayleigh peak intensity is 10^5 times the longitudinal Brillouin doublet. The free spectral range (FSR) is 59.3 GHz. (b) 90° VH scattering. Rayleigh is three times smaller in this polarization than in VV. Brillouin peaks are forbidden.

a crystal by focusing a microscope through the crystal onto its back surface and then translating the crystal with a micrometer to focus on the front surface. The Brillouin frequency was calibrated by comparison with the well-known Brillouin spectra of pure fused silica.[17]

This comparison also allowed us to determine the intensity of peaks in $RbAg_4I_5$ relative to fused silica and determine absolute scattering cross sections. The Rayleigh ratio is defined to be the cross section per unit solid angle of scattered light for a unit volume of scatterer. The Rayleigh ratio of one longitudinal Brillouin component is given by[18]

$$R = \pi^2 K T n^8 P_{12}^2 / 2\rho v_q^2 \lambda_s^4 , \tag{2}$$

where K is Boltzmann's constant, T is the absolute temperature, λ_s is the vacuum wavelength of scattered light, ρ is the density, and P_{12} is the appropriate component of the Pockels' tensor for the scattering geometry in this experiment. The calculated value for fused silica is $R = 0.57\times10^{-7}$ cm^{-1} at room temperature using[19,20] $\rho = 2.2$ g/cm^3 and $P_{12} = 0.27$. We find

$$R = 2\times10^{-6}\ cm^{-1} \tag{3}$$

for $RbAg_4I_5$ at 95°C. We then determine

$$|P_{12}| = 0.15 \pm 0.03 \tag{4}$$

using the value[16] $\rho = 5.384$ g/cm^3. The results in Eqs. (3) and (4) include corrections for changes in internal solid angle due to refraction[18] and transmission losses at the surfaces.

The Brillouin peak has a width that is apparently equal to the 1.2 GHz instrumental width. Because of noise in the experimental data, we estimate that the true Brillouin width is no greater than 0.3 GHz.

The polarized Rayleigh peak shown in Fig. 2(a) has nearly 10^5 times as much intensity as the Brillouin line. Its Rayleigh ratio is therefore approximately 0.14 cm^{-1}. The value for the depolarized peak is 0.05 cm^{-1}, but the apparent leakage of longitudinal Brillouin light into *VH* polarization seen in Fig. 2(b) suggests that much of the depolarized Rayleigh peak is also leakage. A large Rayleigh ratio implies noticeable attenuation of the laser beam, due to scattering. The resulting attenuation coefficient τ, called the "turbidity," appears in the expression for the intensity of light that has traveled a distance x in a medium:[18]

$$I(x) = I_0 e^{-\tau x} . \tag{5}$$

The turbidity is related to the Rayleigh ratio by the expression[18]

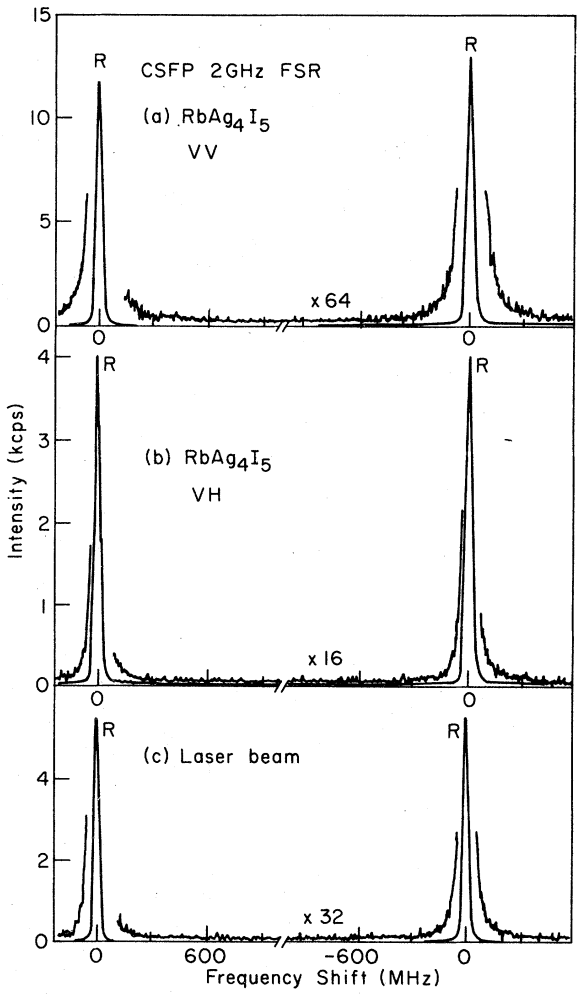

FIG. 3. CSFP data of $RbAg_4I_5$ in 90° scattering for (a) *VV* polarization and (b) *VH* polarization. (c) Anodized aluminum diffuse reflector shows instrument function. The grating-monochromator "filter" was set for 1 cm^{-1} bandpass. The free spectral range was 2 GHz.

$$R = 3\tau/8\pi . \tag{6}$$

The measured Rayleigh ratio implies that the turbidity is 1.2 cm^{-1} for our sample. This value is consistent with the visual observation of a diffuse glow and some attenuation in the crystal when illuminated with laser light.

The only temperature-dependent effect observed was an irreproducible time-dependent increase in the Rayleigh intensity by as much as an order of magnitude after as little as 10 min exposure to laser light at a sample temperature of 32°C. This effect worsened at lower temperatures and hence no measurements were made below 32°C.

The transverse Brillouin peak in $RbAg_4I_5$ was either too weak or too close to the Rayleigh line to be observed.

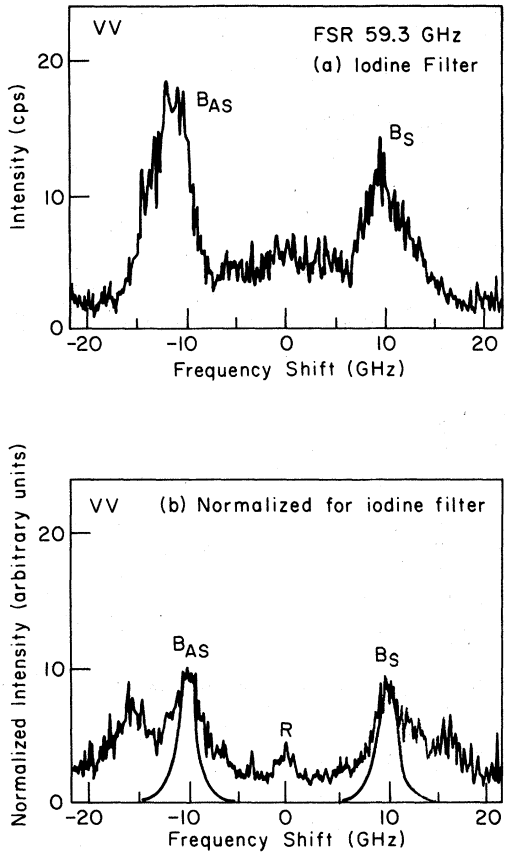

FIG. 4. Single-pass PPFP data of $RbAg_4I_5$ with iodine filter. 90° *VV* scattering. 59.3-GHz FSR. (a) Raw data. (b) Normalized data, divided by iodine spectrum. The spectra beyond ±13 GHz are unreliable because the filtering action of the grating monochromator reduced the signals in both the "raw" spectrum in (a) and the iodine transmission spectrum to low values. Smooth curves are calculated Brillouin peaks.

B. Confocal spherical Fabry-Perot

Figure 3 shows the very high resolution measurement of the "elastic" Rayleigh peak. The peak is very nearly of instrumental width (30 MHz), and we estimate that the peak's true width cannot exceed 10 MHz. Despite the high contrast of 6000, the data show no broader, inelastic Rayleigh components of lesser intensity. The inelastic Rayleigh components discussed below in Secs. III C and III D and the Brillouin doublet already discussed are expected to contribute only a broad background of unobservably low intensity to this measurement.

C. Fabry-Perot interferometer with iodine cell

Figure 4 shows the Brillouin spectra distorted by transmission though an iodine cell and its normalization obtained by dividing by the transmission function of the iodine cell.[21] This transmission function was measured using a white-light source in place of a sample. The Brillouin peaks are broader than those shown in Fig. 2 because of the smaller single-pass interferometer finesse of 35 and the spread in phonon wave vector[22] that results from the larger collection angle when the full PPFP mirror aperture is used in the singly passed mode. The smooth curves are theoretical ones calculated by taking both effects into account. As we expected from the CSFP data, the iodine cell, which has a 700 MHz instrumental full width at half maximum, removed the very intense, narrow "elastic" Rayleigh peak. All that remains is a rather broad central component of uncertain line shape whose integrated intensity we estimate to be twice the Brillouin intensity, assuming the broad component to be a Lorentzian with a half width at half maximum of roughly 9 GHz. This feature was revealed repeatedly in other scans, not shown here, with different free spectral ranges.[23] It will be called the "narrow dynamic central component."

There are several arguments underlying the claim that there is inelastic light between 0–10 GHz in the spectra of Fig. 4. First, the mere appearance of light in this frequency region is evidence for this peak, since the elastic peak is eliminated. Second, the spectrum taken with higher resolution has modulations corresponding to the iodine transmission function, proving it is inelastic light, not stray laser light.[23] Third, normalization of spectra by dividing by the iodine filter can improve the appearance and symmetry of part of the data. Fourth, the demonstration in Sec. III A that the Brillouin peaks are instrumental in width removes them as contributors to inelastic light. Fifth, the high resolution reduces the broad 1.4± 0.2 cm^{-1} central component discussed in Sec. III D to a negligible intensity, so it cannot be the source of the inelastic spectrum in this frequency range.

The Stokes Brillouin peak in Fig. 4(a) is less intense than the anti-Stokes peak because of an iodine absorption line that was observed very close to it, just beyond 10 GHz. The relative intensities of Stokes and anti-Stokes lines was found to be highly sensitive to the tuning of the laser to the peak of the absorption of the iodine filter. This was also a problem with the data to be shown below in Fig. 5. Additional distortion of the spectra of Fig. 4 results from drift of the unstabilized PPFP.

D. Double grating monochromator with iodine cell

Figure 5 shows the Rayleigh peak and two Brillouin peaks distorted by the iodine cell taken with

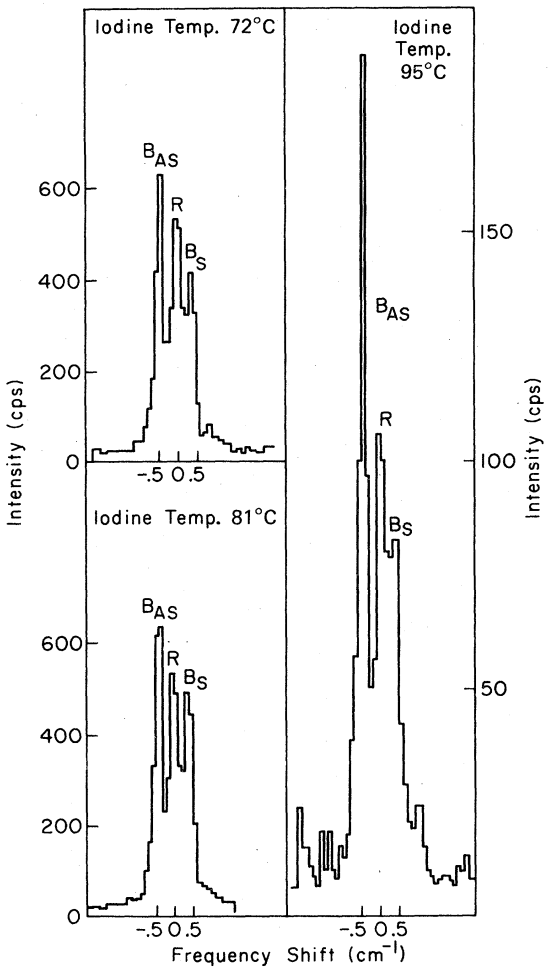

FIG. 5. Resolution of the Brillouin-doublet and Rayleigh peak in $RbAg_4I_5$ with a double monochromator and an iodine filter. 90° $VV+VH$ scattering.

the double monochromator, using 0.25 cm^{-1} resolution. A stepping motor translated the monochromator setting in 0.1-cm^{-1} steps. This was coarse enough to contribute to the distortion of the spectra.

We have used two properties of the iodine filter to prove to ourselves that line R in Fig. 5 is indeed a narrow inelastic Rayleigh peak. First we found that at 95°C the iodine filter attenuates the laser line by a factor of 5×10^8 more than at 22°C.[23] We found the Rayleigh peak at 22°C to be 7×10^8 counts/sec; if completely elastic the peak should therefore be reduced to 1.5 counts/sec at a filter temperature of 95°C. Instead it was 100 counts/sec. The second proof follows from the fact that the attenuation of the cell increased by a factor of 3 for every 5°C rise in its temperature, but the intensity of line R was found by measurements not shown in Fig. 5 to decrease by only a factor of 2 during a 25°C change in filter temperature.[23]

Figure 6 shows an attempt to isolate the central component by subtracting the Brillouin peaks from a spectrum (not the same one as Fig. 5) under the assumption that the Brillouin peaks are symmetric. The width and integrated intensity of this central component are quite consistent with values determined with the PPFP interferometer and iodine cell.

Figure 7(a) shows a lower resolution scan (0.6 cm^{-1} width) that reveals a broader Rayleigh component visible out to 10 cm^{-1}. Shown in Fig. 7(b) is the white light transmission of the iodine cell and the resulting corrected spectrum is shown in Fig. 8. The Brillouin doublet now merges with the narrow inelastic component because of the lower resolution. If these low-frequency features and a constant baseline, (representing the low-frequency part of the 20-cm^{-1} Raman peak) are subtracted from the data, the remaining broad peak fits a Lorentzian of halfwidth 1.3± 0.2 cm^{-1} or roughly 40± 6 GHz.[23] The quoted uncertainty depends on how the subtraction is performed near the central part of the spectrum. The wings are unaffected. The integrated intensity is about one half the Brillouin intensity. If this broad peak were studied with an interferometer of 1.2 GHz bandpass, such as that used to obtain the data in Fig. 2, its intensity would be only a few percent of the Brillouin peak intensity, and it would not be observable above the true background.

We have not made a careful study of the polarization properties of the two inelastic central components. The data that are available indicate that the polarized and depolarized spectra have the same shape. The VV $(A_1+\frac{4}{3}E)$ component of the narrow inelastic central peak seems to be about 40% more intense than the VH (T_2) component.[23] A study of the symmetry properties of the tail of the wide component at 4 cm^{-1} suggested that the strongest component was T_2, and the next strongest was E.[24]

IV. SUMMARY OF EXPERIMENTAL RESULTS

The first observations of the Brillouin spectra in $RbAg_4I_5$ were performed. The longitudinal acoustical phonon appears at a frequency shift of 10 GHz for 90° scattering with excitation by a 5145-Å line. The result is in agreement with the measured sound velocity for a value of index of refraction of 2.1; this value was verified by direct measurement.

The linewidth was less than instrumental and therefore less than 0.3 GHz according to the triple-pass Fabry-Perot data. The transverse acoustical phonon was not observed, apparently

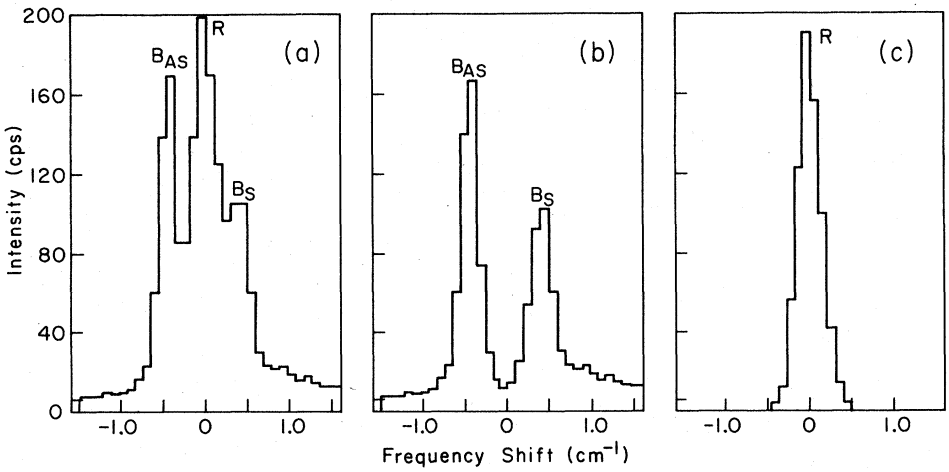

FIG. 6. (a) Triple peak of $RbAg_4I_5$. (b) Analysis of peaks into Brillouin doublet and (c) Rayleigh component.

due to its weakness and low frequency.

The broad central peak in $RbAg_4I_5$ has a Lorentzian shape and was studied from 1 to 10 cm^{-1}. Its integrated intensity indicates a Rayleigh ratio of 9×10^{-7} or about half that of the Brillouin peak. Its halfwidth is 1.3 ± 2 cm^{-1} or 40 ± 6 GHz.

A narrower Rayleigh peak appears in the Fabry-Perot data. Its intensity is about $\frac{1}{4}$ that of the Brillouin peaks. In the double monochromator data its intensity is $\frac{1}{2}$ that of the Brillouin peaks. Its width is difficult to determine due to its weak intensity in the former experiment and its narrowness in the latter experiment. In addition it is distorted by the effects of the iodine filter. It appears to have an integrated intensity twice that of the Brillouin peak, or a Rayleigh ratio of about $(4\pm1)\times10^{-6}$ cm^{-1}. Actually, the interferometer indicates a value at the upper limit, and the monochromator indicates the lower limit. The half width of 0.3 ± 0.1 cm^{-1} or 9 ± 3 GHz is indicated by both measurements.

The last remaining feature is the apparently static and extremely intense Rayleigh peak that is totally removed by the iodine filter. Its intensity is 10^5 greater than that of any other observed feature. The iodine filter demonstrates the absence of any features broader than 1 GHz other than the weak ones already described. The Rayleigh peak has a Rayleigh ratio of 0.14 cm^{-1} for *VV* polarization and 0.05 cm^{-1} for *VH* polarization. Its width is less than 10 MHz, according to spherical Fabry-Perot measurements, and no features greater than 10 MHz were observed with an instrumental contrast of 6000. Although its intensity was constant for many regions of the crystal for long time intervals, it did change unpredictably near the disproportionation temperature (27°C). Most spectra were run at 90°C

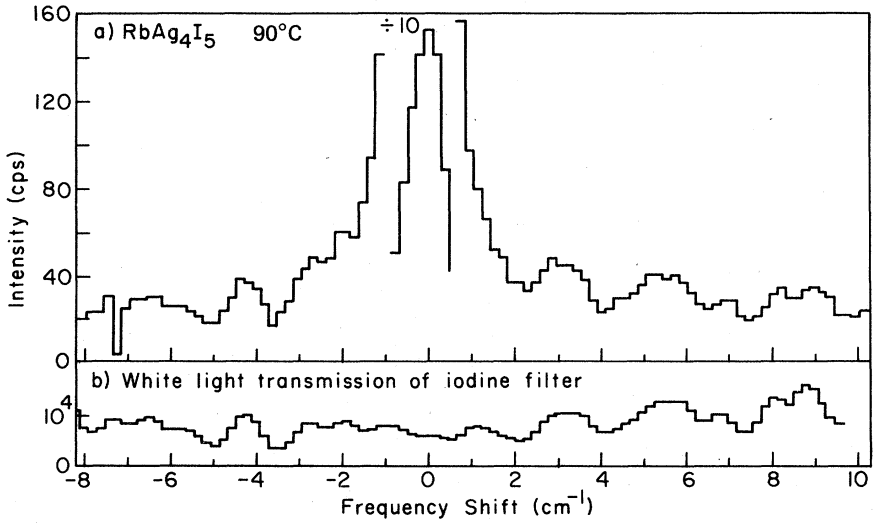

FIG. 7. (a) Stokes and anti-Stokes Raman spectra of $RbAg_4I_5$ with the unresolved central peak (*VV* + *VH*). (b) Iodine filter (temperature 96 °C)transmission of white light.

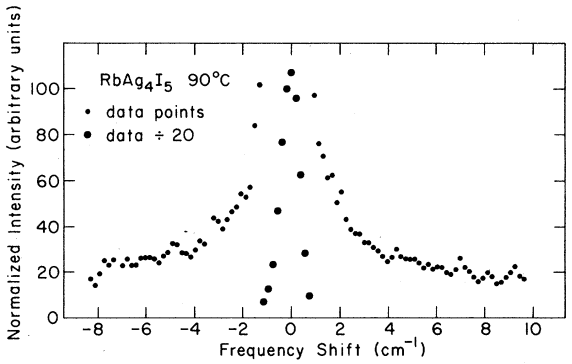

FIG. 8. Raman spectra of $RbAg_4I_5$ corrected for iodine-filter transmission function $(VV+VH)$.

where the crystal is relatively stable for moderate laser powers (1–10 mW).

V. DISCUSSION OF RAYLEIGH PEAKS

We believe that at least one of the two quasielastic peaks is due to the diffusive motion of the silver ions. The other peak could also be due to diffusive motion. Another possibility is that it could have the same origin as the "broad" inelastic peak observed by Lyons and Fleury.[24] Those authors found their peak to have a width and an intensity proportional to temperature. They were uncertain about its origin but speculated that it is caused by phonon difference processes. It is unfortunate that we were unable to study the inelastic peaks in $RbAg_4I_5$ over a sufficiently wide temperature range to allow a determination of their temperature dependence.

We return to the possibility that both of our quasielastic peaks might be due to diffusion. A Ag^+ ion will clearly have a different polarizability on two different inequivalent sites. On two equivalent sites, say two type-II sites, in the same unit cell, the orientational environments are different, giving rise to different directions for the principal axes of the polarizability tensor. During an ion's flight between two sites, its polarizability will take on values different from either its initial or final values.

Thus, if the time of flight t_f between sites is noticeably shorter than the dwell time t_d at a site, we expect two time scales for the fluctuations in the polarizability. This should give rise to a superposition of two central peaks, whose widths may be estimated from the uncertainty principle:

$$\Delta f_b \cong (2\pi t_f)^{-1}, \tag{6a}$$

$$\Delta f_n \cong (2\pi t_d)^{-1}. \tag{6b}$$

Specific models of relaxation modes will give a more precise expression for the width of the narrow component than Eq. (6b), but the data do not warrant such a treatment. There should be 56 zero wave-vector relaxation modes in $RbAg_4I_5$. One of these is the "equilibrium mode" with zero relaxation rate (see the Appendix). There should be 13 Raman-active relaxation modes: $2A_1+4E+7T_2$.[25]

One would need specific models for the change in polarizability during the flight of a silver ion to be able to improve on the estimate Eq. (6a) for the width of the broad component. An alternate approach has been taken by Geisel and collaborators,[26] who have treated light scattering by a particle undergoing Brownian motion in a sinusoidal potential. The polarizability is considered to be a sinusoidal function of position. Such a theory does not require the assumption that $t_f \ll t_d$.

Still assuming that both the 9 and 40 GHz (half width) inelastic central peaks are due to diffusion, we have at least two choices. One is the identification of the two peaks with dwelling and flying and hence with the two time scales in Eq. (6). We then obtain the estimates

$$t_d = 18 \text{ psec}, \tag{7a}$$

$$t_f = 4 \text{ psec}. \tag{7b}$$

As a check on the consistency of this identification of the narrow component with t_d we use the relation

$$D = a_0^2/6t_d \tag{8}$$

to estimate t_d. Depending on the site, the intersite distance a_0 varies from 1.7 to 1.9 Å.[16] Assuming $a_0 = 1.8$ Å and using $D = 3.7\times10^{-6}$ cm²/sec, the value for D at 90°C implied by Bentle's experimental results,[27] we find

$$t_d = 14.6 \text{ psec}. \tag{9}$$

The agreement between (7a) and (9) suggests that the identification of the narrow peak with dwelling is correct. A similar identification using a specific relaxation mode has recently been made for α-AgI.[11,26]

The dwelling-flying picture implies that the intensities of the two central components should be equal to the mean-square fluctuation in polarizability associated with the motion they represent weighted by the fraction of all ions undergoing such motion. These weighting factors should be proportional to t_d and t_f. Since we found that the narrower component had about four times as much integrated intensity as the broader component, and since this ratio is close to the ratio of t_d to t_f, the dwelling-flying model implies that the

mean-square change in polarizability at two different sites is about equal to the change during flight between two sites.

The second choice is to identify the 9 and 40 GHz central peaks with two groups of relaxation modes whose rates differ by a factor of 4.5, and to assume that "flying" produces too weak a central peak to be observed. To test the reasonableness of this choice of dwelling-dwelling, we quote an approximate result from the theory of relaxation modes. Assuming independent particles diffusing in a cubic lattice having r sites per unit cell we show in the Appendix that the mean relaxation rate obeys the approximate result

$$\bar{\nu} \equiv r^{-1} \sum_{\lambda=1}^{r} \nu(k=0,\lambda) \approx t_d^{-1} \equiv \frac{6D}{a_0^2} \tag{10}$$

The summand in Eq. (10) is the frequency of the λth relaxation mode of zero wave vector. Equation (10) rests upon the following three assumptions: (i) All hopping distances are equal to a_0; (ii) There are no direct hops from a given site in one unit cell to the same site in another unit cell; and either (iii a) all sites have the same occupation probability or (iii b) all sites have the same diagonal element of the jump rate matrix. Assumptions (i) and (ii) are reasonable for $RbAg_4I_5$. (iii a) is false, but (iii b) may not be unreasonable. The relaxation rate of a mode divided by 2π gives the frequency at the half width at half maximum for that mode (Eq. A9c), so that the average frequency half width of all 56 relaxation modes in $RbAg_4I_5$ should obey Eq. (A23):

$$\langle \Delta f \rangle = \bar{\nu}/2\pi \approx 1/2\pi t_d = 11 \text{ GHz}. \tag{11a}$$

We have used Eq. (9) for the numerical estimate. If we assume that all equilibrium jump rates between accessible pairs of sites are the same (Eq. A15a), then Eq. (A24b) holds, leading to the result

$$\langle \Delta f \rangle = 13 \text{ GHz}. \tag{11b}$$

It is perhaps unlikely, but not impossible, that there would be groups of relaxation modes with Δf's of 9 and 40 GHz such that the average of all Δf's is 11–13 GHz.

To summarize, we believe a reasonable assignment of the 9-GHz Rayleigh peak is to "dwelling." We prefer the assignment of the 40-GHz peak to "flying," but recognize that it might be of nondiffusive origin or that it might also be due to "dwelling."

The origin of the intense static peak remains unknown. It is a matter of speculation whether it is due to defects in the optical quality of the crystal or due to intrinsic properties of the crystal, that is, of truly molecular origin. It is difficult to imagine any molecular mechanisms of sufficient strength this far (155°C) away from the 208-K phase transition. One might assign this peak to the motions of the walls of domains of silver ions—if such domains exist. One can speculate that at 32 K, near the 27 K disproportionation temperature the crystal was decomposing slightly into the other nearby phases indicated on the phase diagram.[4] It is possible that such phenomena occured at 90°C also, only more slowly.

ACKNOWLEDGMENTS

This research was supported by the National Science Foundation under Grant No. DMR 77-04382 and Contract No. DMR 76-01058. We thank T. H. Wood for developing the computer-controlled stabilization system for the Fabry-Perot interferometer.

APPENDIX: RELAXATION MODES ON A LATTICE

Relaxation processes of hydrogen atoms in a lattice of translationally inequivalent sites have been considered by Rowe *et al.*,[28] but they assumed that each type of site was occupied with equal probability, an assumption that is not valid for Ag^+ ions in $RbAg_4I_5$. Our purpose here is (i) to develop briefly the theory in the case of unequal probability and (ii) to derive an approximate relation between the frequencies of the "optical" relaxation modes (i.e., those that have nonzero rate for zero wave vector) and the diffusivity.

Let i ($i=1,\ldots,r$) denote the site index on a bravais lattice generated by a set of primitive displacement vectors $\{\vec{L}\}$. The occupation number $N_{iL}(t)$ is a random variable that describes the occupancy of site i in cell L. It has a mean value of P_i, the equilibrium occupation probability for site i. Let α_i be the scalar product of the polarizability tensor for a silver ion at site i with incident and scattered photon polarization unit vectors. Then the polarizability operator for the entire crystal is

$$\alpha(t) = \sum_{iL} \alpha_i N_{iL}(t) \tag{A1}$$

and the light scattering cross section for the crystal is proportional to

$$S_\alpha(\omega) = \frac{1}{2\pi} \int_{-\infty}^{\infty} \langle\langle \alpha(t)\alpha(0) \rangle\rangle e^{i\omega t} dt. \tag{A2}$$

In Eqs. (A1) and (A2) we have set the wave-vector transfer equal to zero. Equations (A1) and (A2) require knowledge of the correlation function $\langle\langle N_{iL}(t) N_{jL'}(0) \rangle\rangle$, which is an even function of t that obeys the boundary conditions

$$\langle N_{iL}(0)N_{jL'}(0)\rangle = P_i \delta_{ij}\delta_{LL'}, \tag{A3a}$$

$$\langle N_{iL}(\infty)N_{jL'}(0)\rangle = P_i P_j . \tag{A3b}$$

Let $C_{ij}(L-L')$ be the hopping probability per unit time for an ion to hop from site (i,L) to site (j,L'). Since the system is translationally invariant, it depends on the variable $\vec{L}-\vec{L}'$. For $t>0$ we find

$$\frac{d}{dt}\langle N_{iL}(t)N_{j'M}(0)\rangle = \sum_{jL'} C_{ij}(L-L')\langle N_{jL'}N_{j'M}(0)\rangle . \tag{A4}$$

Equation (A3b) implies the *equilibrium condition*

$$\sum_{jL'} C_{ij}(L-L')P_j = 0 . \tag{A5}$$

The principle of microscopic *detailed balance* says

$$C_{ij}(L-L')P_j = C_{ji}(L'-L)P_i . \tag{A6}$$

The symmetric matrix

$$R_{ij}(L-L') = C_{ij}(L-L')(P_j/P_i)^{1/2} \tag{A7}$$

will have normalized eigenvectors of the form

$$E_i(L) = e_i(k\lambda)e^{i\vec{k}\cdot\vec{L}_i}/\sqrt{N}, \tag{A8a}$$

where

$$\vec{L}_i = \vec{L} + \vec{a}_i , \tag{A8b}$$

where $\vec{a}_i$ is the location of the ith site within a unit cell, and where

$$\sum_{i=1}^{r} [e_i(k\lambda)]^2 = 1 . \tag{A8c}$$

The eigenvalues $\nu(k\lambda)$ are the negatives of the relaxation rates for each relaxation mode.

We then find that $S_\alpha(\omega)$ is a sum of Lorentzians

$$S_\alpha(\omega) = N\pi^{-1}\sum_{\lambda} \frac{\nu(0\lambda)[\alpha(\lambda)]^2}{[\nu(0\lambda)]^2+\omega^2}, \tag{A9a}$$

where

$$\alpha(\lambda) = \sum_{i=1}^{r} \sqrt{P_i}\, E_i(0\lambda)\alpha_i . \tag{A9b}$$

In (A9a) N is the number of unit cells in the crystal. Raman-active relaxation modes λ will give a nonzero result for $\alpha(\lambda)$. Equation (A9a) describes a superposition of Lorentzians centered at zero frequency whose half width at half maximum (half width) as a function of frequency is given by

$$\Delta f(\lambda) = \nu(0\lambda)/2\pi . \tag{A9c}$$

The equilibrium condition (A5) implies that the eigenvector

$$E_i(L) = N^{-1/2}e_i(k=0,1) = \sqrt{P_i/Nn} \tag{A10a}$$

has eigenvalue zero. Here

$$n = \sum_{i=1}^{r} P_i . \tag{A10b}$$

For small but nonzero k this "equilibrium mode" has eigenvalue

$$\nu(k,1) = \sum_{ijM} C_{ij}(M)(P_j/n)\, e^{-i\vec{k}\cdot(\vec{M}+\vec{a}_i-\vec{a}_j)} .$$

We expand the exponential in a series in k. The first-order term can be shown to vanish by use of the detailed balance condition (A6). The zeroth- and second-order terms may be combined by using the equilibrium condition to obtain

$$-\nu(k,1) = \vec{k}\cdot\vec{D}\cdot\vec{k}, \tag{A11}$$

where the diffusivity tensor is, in Cartesean coordinates,

$$D_{\alpha\beta} = \frac{1}{2}{\sum_{ijM}}' C_{ij}(M)\frac{P_j}{n}(M_\alpha + a_{i\alpha} - a_{j\alpha})(M_\beta + a_{i\beta} - a_{j\beta}) . \tag{A12a}$$

For a cubic crystal, $D_{\alpha\beta} = D\delta_{\alpha\beta}$, with

$$D = \frac{1}{6}{\sum_{ijM}}' C_{ij}(M)\frac{P_j}{n}|\vec{M}+\vec{a}_i-\vec{a}_j|^2 . \tag{A12b}$$

The prime in Eq. (A12) means that $i\neq j$ when $M=0$.

Let us now assume that all the jump distances $|\vec{M}+\vec{a}_i-\vec{a}_j|$ are the same and equal to a_0. Then we may use the equilibrium condition (A5) in (A12b) to obtain

$$D = a_0^2/6t_d , \tag{A13a}$$

where the time t_d obeys

$$t_d^{-1} \equiv \sum_{i=1}^{r} \frac{-C_{ii}(0)P_i}{n} . \tag{A13b}$$

Some special cases of Eq. (A13) will be of interest. If all sites have equal occupancy P_i, then

$$P_i/n = r^{-1} \tag{A14a}$$

and

$$t_d^{-1} = -r^{-1}\sum_{i=1}^{r} C_{ii}(0) . \tag{A14b}$$

Another special case occurs if all the equilibrium jump rates between accessible pairs of sites are the same, i.e., if

$$C_{ij}(M)P_j = A \tag{A15a}$$

for all neighboring pairs of sites. Then

$$C_{ii}(0)P_i = -Z_i A , \tag{A15b}$$

where Z_i is the number of neighbors to site i. We find

$$t_d^{-1} = A\sum_{i=1}^{r} \frac{Z_i}{n} . \tag{A15c}$$

Use of (A10) in (A8) implies that the eigenvalues for finite k are those of the Hermitian matrix

$$r_{ij}(\vec{k}) = \sum_M R_{ij}(M) e^{-i\vec{k}\cdot(\vec{M}+\vec{a}_i-\vec{a}_j)}. \tag{A16}$$

The matrix

$$r_{ij}(0) = \sum_M R_{ij}(M) \tag{A17}$$

plays the role of R_{ij} in Ref. 8. The trace of this matrix gives minus the sum of the $k=0$ relaxation rates

$$-\sum_{\lambda=1}^{r} \nu(k=0,\lambda) = \sum_{i=1}^{r} \sum_M C_{ii}(M). \tag{A18}$$

The sum on the left-hand side includes the contribution of the equilibrium mode for which $\nu = 0$.

We now assume that there are no direct hops between site i in one unit cell and site i in another unit cell. This implies

$$C_{ii}(M) = 0 \quad \text{unless } M = 0, \tag{A19}$$

and (A18) becomes

$$-\sum_{\lambda=1}^{r} \nu(k=0,\lambda) = \sum_{i=1}^{r} C_{ii}(0).$$

Introducing a mean relaxation rate $\bar{\nu}$

$$\bar{\nu} \equiv r^{-1} \sum_{\lambda=1}^{r} \nu(k=0,\lambda), \tag{A20}$$

we find

$$\bar{\nu} = -r^{-1} \sum_{i=1}^{r} C_{ii}(0) \tag{A21}$$

Using the assumption that P_i is independent of i, we find using Eq. (A15b) that

$$\bar{\nu} = t_d^{-1} \tag{A22a}$$

or that

$$D = a_0^2/6t_d = \tfrac{1}{6} a_0^2 \bar{\nu} \tag{A22b}$$

This implies, according to Eq. (A9c), that the average half width, as a function of frequency, of all relaxation modes obeys the relation

$$\langle \Delta f \rangle \equiv \bar{\nu}/2\pi = 6D/2\pi a_0^2. \tag{A23}$$

Using the assumption of equal equilibrium jump rates (A15b) we find

$$\bar{\nu} = \frac{A}{r} \sum_i \frac{Z_i}{P_i} \tag{A24a}$$

or, using (A15c),

$$\bar{\nu} = \frac{t_d^{-1} \sum_i (Z_i/P_i)}{r \sum_i (Z_i/n)}. \tag{A24b}$$

---

*Present address: Rocketdyne Division, Rockwell International, Canoga Park, Calif. 91304.

†Present address: Defense Systems Division, Northrop Corporation, 175 W. Oakton Street, Des Plaines, Ill. 60018.

[1] J. N. Bradley and P. D. Greene, Trans. Faraday Soc. 62, 2069 (1966); 63, 424 (1967); B. B. Owens and G. R. Argue, Science 157, 308 (1967).

[2] K. Funke, Prog. Solid State Chem. 11, 345 (1976).

[3] (a) S. Geller, in *Fast Ion Transport in Solids*, edited by W. van Gool (North-Holland, Amsterdam, 1973), p. 607; (b) S. Geller, Phys. Rev. B 14, 4345 (1976); (c) S. Geller, in *Superionic Conductors*, edited by G. D. Mahan and W. L. Roth (Plenum, New York, 1976), p. 171.

[4] B. B. Owens, in Ref. 3 (a), p. 593.

[5] L. Heyne, in Ref. 3 (a), p. 130.

[6] D. A. Gallagher and M. V. Klein, J. Phys. C 9, L687 (1976).

[7] D. A. Gallagher and M. V. Klein (unpublished).

[8] M. V. Klein, in *Light Scattering in Solids*, edited by M. Balkanski, R. C. C. Leite, and S. P. S. Porto (Flammarion, Paris, 1976), p. 351.

[9] B. A. Huberman and R. M. Martin, Phys. Rev. B 13, 1498 (1976).

[10] M. B. Salamon, Phys. Rev. B 15, 2236 (1977).

[11] G. Winterling, W. Senn, M. Grimsditch, and R. Katiyar in Lattice Dynamics Conference, 1977) (unpublished).

[12] M. R. Manning, C. J. Venuto, and D. P. Boden, J. Electrochem. Soc. 118, 2031 (1971).

[13] T. H. Wood, Rev. Sci. Instrum. 49, 790 (1978).

[14] G. E. Devlin, J. L. Davis, L. Chase, and S. Geschwind, Appl. Phys. Lett. 19, 138 (1971).

[15] L. J. Graham and R. Chang, J. Appl. Phys. 46, 2433 (1975).

[16] S. Geller, Science 157, 310 (1967).

[17] W. F. Love, Phys. Rev. Lett. 31, 822 (1973).

[18] P. E. Schoen and H. Z. Cummins, in *Light Scattering in Solids*, edited by M. Balkanski (Flammarion, Paris, 1971), p. 460.

[19] Amersil Inc., Optical Fused Quartz and Fused Silica, Hillside, N. J. 1973, (unpublished catalog)

[20] D. A. Pinnow, in *Handbook of Lasers*, edited by R. J. Pressley (Chemical Rubber, Cleveland, 1971), p.478.

[21] K. B. Lyons and P. A. Fleury, J. Appl. Phys. 47, 4898 (1976).

[22] G. E. Durand and A. S. Pine, IEEE J. Quantum Electronics 4, 523 (1968).

[23] Robert A. Field, Ph.D. thesis (University of Illinois at Urbana-Champaign, 1978) (unpublished).

[24] K. B. Lyons and P. A. Fleury, Phys. Rev. Lett. 37, 161 (1976).

[25] David A. Gallagher, Ph.D. thesis (University of Illinois at Urbana-Champaign, 1978) (unpublished).

[26] T. Geisel, Solid State Commun. 24, 155 (1977); W. Dieterich, T. Geisel, and I. Peschel, Z. Phys. B 29, 5 (1978).

[27] G. G. Bentle, J. Appl. Phys. 39, 4036 (1968).

[28] J. M. Rowe, Kurt Sköld, and H. E. Flotow, J. Phys. Chem. Solids 32, 41 (1971).